Chemical Engineering Science 192 (2018) 972–980

Contents lists available at ScienceDirect

Chemical Engineering Science

journal homepage: www.elsevier.com/locate/ces

Modeling the transport and retention of polydispersed colloidal suspensions in porous media

Scott A. Bradford [a,*], Feike J. Leij [b]

[a] US Salinity Laboratory, USDA, ARS, Riverside, CA, United States
[b] Department of Civil Engineering and Construction Engineering Management, California State University, Long Beach, CA 90840-5101, United States

HIGHLIGHTS

- A new model for the fate of polydispersed colloid suspensions in porous media.
- Polydispersed suspensions become more uniform with increasing transport distance.
- Retention profiles were mainly influenced by polydispersed suspension at the inlet.
- Aggregation produces breakthrough curves with a "ripening" shape.
- Hyper-exponential retention profiles occurred with aggregating suspensions.

ARTICLE INFO

Article history:
Received 16 April 2018
Received in revised form 17 June 2018
Accepted 17 August 2018
Available online 18 August 2018

Keywords:
Colloids
Nanoparticles
Aggregation
Transport
Polydispersed
Modeling

ABSTRACT

Colloid suspensions commonly exhibit a distribution of sizes, but most transport models only consider a single colloid size. A mathematical model was therefore developed to describe the advective and dispersive transport and first-order retention and release of a stable or aggregating polydispersed colloid suspension in porous media. The colloid size distribution was described using a unimodal or a bimodal lognormal probability density function (PDF), and Brownian aggregation was considered by making lognormal PDF parameters a function of time. Filtration theory was used to predict the retention rate coefficients for the various colloid sizes. The amount of retention for a stable polydispersed suspension was highly dependent on the colloid size distribution parameters, especially for a bimodal lognormal PDF. Increasing the distribution variance produced hyper-exponential retention profiles and an increase or a decrease in colloid retention depending on whether the medium colloid size was close to the optimum size for transport. Aggregation produced a similar decrease in the breakthrough concentrations with injection time as ripening, especially when the sticking efficiency was low. Aggregation effects were much more pronounced at higher input concentration levels, which also produced retention profiles that were increasingly hyper-exponential. Simulation results indicate that the colloid size distribution of stable and aggregating polydispersed suspensions always becomes more uniform and approaches the optimum transport size with increasing distance, suggesting that consideration of polydispersed suspensions is of primary importance near the injection surface.

Published by Elsevier Ltd.

1. Introduction

Most research studies and mathematical models to describe colloid (microorganisms, clays, nanoparticles, etc.) transport and fate in porous media have been developed for monodispersed colloidal suspensions (Schijven and Hassanizadeh, 2000; Bradford et al., 2014). In reality, natural suspensions exhibit a wide distribution of colloid sizes (Ryan and Elimelech, 1996; Filella et al., 1997; Bradford et al., 2006; Alem et al., 2013, 2015). The colloid size distribution reflects the variation in the initial conditions, different rates of retention and/or release of specific colloid sizes, and/or aggregation. The colloid size has a strong influence on the rates of retention, release, and aggregation. For example, the mass transfer rate of colloids to the solid water interface (SWI) and the aggregation rate are strongly dependent on the colloid size (Elimelech et al., 2013; Messina et al., 2015). Consequently, the transport and retention behavior of a polydispersed colloid suspension cannot be determined simply from the mean colloid size (Vigneswaran et al., 1990).

* Corresponding author.
E-mail address: Scott.Bradford@ars.usda.gov (S.A. Bradford).

https://doi.org/10.1016/j.ces.2018.08.037
0009-2509/Published by Elsevier Ltd.

A number of studies have demonstrated that the size distribution of colloid suspensions can change during transport (e.g., Vigneswaran et al., 1990; Mackie and Zhao, 1999; Bradford et al., 2006; Wiesner and Bottero, 2007; Klaine et al., 2008; Fang et al., 2009; Chatterjee et al., 2010; Solovitch et al., 2010; Bian et al., 2011; Chen et al., 2011; Jiang et al., 2012; Wang et al., 2012a, 2012b; Alem et al., 2013, 2015; Taghavy et al., 2015). Differences in the retention behavior for the individual size classes and/or aggregation will produce changes in the colloid size distribution during transport. Jiang et al. (2012) found that ZnO nanoparticles aggregated during transport, and that the retained aggregate size decreased with transport distance. Wang et al. (2012a) and Solovitch et al. (2010) reported that the average size of TiO_2 nanoparticles increased dramatically after passing through sand columns. Conversely, Chen et al. (2011) and Wang et al. (2012b) found that the size of TiO_2 and Alizarin red S labeled hydroxyapatite nanoparticles decreased after transport through sand columns. Differences in the size distribution of colloids with transport have been associated with observed non-exponential profiles of retained colloids that are not consistent with filtration theory predictions (Chatterjee and Gupta, 2009; Chen et al., 2011; Jiang et al., 2012; Wang et al., 2012b).

A limited number of models have been developed to simulate the transport and retention of polydispersed colloid suspensions (Chang and Vigneswaran, 1990; Mackie and Zhao, 1999; Chatterjee and Gupta, 2009; Raychoudhury et al., 2012). The earlier models were designed to examine improvements in long-term wastewater filter performance as a result of retention of a polydispersed colloid suspension (e.g., ripening) (Chang and Vigneswaran, 1990; Mackie and Zhao, 1999). In this work, we consider clean-bed (early-time) retention behavior that is more representative of studies in natural environments with dilute colloidal suspensions. Chatterjee and Gupta (2009) developed a steady-state advective transport and first-order retention model for polydispersed colloid suspensions and demonstrated that it could produce hyper-exponential retention profiles. Chatterjee et al. (2010) applied this model to study the transport of a polydispersed suspension and accounted for the influence of colloid size on the retention coefficient using empirical correlations for the mass transfer coefficient and fitted values of the sticking efficiency. Raychoudhury et al. (2012) simulated the transport, retention, and release of an aggregating colloid suspension by coupling the solution of the transient advective dispersion equation that included first order terms for colloid attachment and detachment with a kinetic aggregation model. Differences in the retention rate coefficient with colloid size were accounted for using filtration theory.

A variety of stochastic models have been used to account for chemical heterogeneity of the colloid population (Tufenkji et al., 2003; Bradford and Toride, 2007). In these works various probability density functions (PDFs) for the colloid attachment coefficient have been utilized (Tufenkji et al., 2003) with joint PDFs for the effect of correlation between parameters (e.g., attachment and detachment coefficients, attachment coefficient and pore-scale velocity distribution, and detachment coefficient and the pore-scale velocity distribution) on colloid transport (Bradford and Toride, 2007). Simulation results demonstrate that the retention profile of retained colloids is highly sensitive to the PDF of the colloid attachment coefficient and/or the correlations between stochastic model parameters. We believe that these stochastic models may be extended to simulate the transport and retention behavior of polydispersed colloid suspensions, although this has not yet been undertaken.

The objective of this research was to develop an improved model to describe the transport and retention of stable or aggregating polydispersed colloid suspensions in porous media. Specific model refinements include consideration of: (i) a variety of PDFs for the colloid size distribution; (ii) aggregating suspensions; (iii) total and size class concentrations in the aqueous and solid phases; and (iv) changes in the colloid size distribution with transport distance. Illustrative simulations are presented to demonstrate the sensitivity of model predictions to various parameter values. Results provide new insight on causes for time dependent breakthrough curves and non-exponential retention profiles, and changes in colloid size distributions during transport, retention, and/or aggregation of polydispersed suspensions under specific physicochemical conditions.

2. Modeling colloid transport and retention

2.1. Monodispersed suspensions

Colloid transport in porous media is frequently described using a one-dimensional advection dispersion equation with terms for first-order retention and release (e.g., Schijven and Hassanizadeh, 2000; Bradford et al., 2014). This approach implicitly assumes a monodispersed suspension of colloids with a given diameter or range in diameter (D_i expressed in nm). When the volumetric water content and flux remain constant in time (steady-state water flow), the aqueous phase colloid mass balance equation is written as:

$$\frac{\partial C_i}{\partial t} = v\lambda\frac{\partial^2 C_i}{\partial z^2} - v\frac{\partial C_i}{\partial z} - k_i C_i + \frac{\rho_b k_{rs}}{\theta} S_i \tag{1}$$

where C_i [NL^{-3}; N and L denote the number of colloids and length, respectively] and S_i [$N\ M^{-1}$; M denotes mass] are the colloid concentration of diameter D_i in the aqueous phase and on the solid phase, respectively, k_i [T^{-1}] is the retention rate coefficient for colloid diameter D_i, k_{rs} [T^{-1}] is the constant colloid release rate coefficient, t [T] is time, z [L] is depth, v is the average pore-water velocity [$L\ T^{-1}$], λ is the dispersivity [L], ρ_b [$M\ L^{-3}$] is the soil bulk density, and θ [–] is the volumetric water content. The corresponding colloid mass balance equation for the solid phase is given as:

$$\frac{\rho_b}{\theta}\frac{\partial S_i}{\partial t} = k_i C_i - \frac{\rho_b k_{rs}}{\theta} S_i \tag{2}$$

The dispersivity was set to $0.1 * L_D$ for all simulations, where L_D [L] is the length of the considered simulation domain. Values for θ and ρ_b were set equal to 0.34 and 1.82 g cm^{-3}, respectively; typical values for a sand (e.g., Schaap et al., 2001).

The CXTFIT code (Toride et al., 1995; Tang et al. 2010) was used for the analytical solution of Eqs. (1) and (2). The initial concentration in the simulation domain was zero, a third-type boundary condition was employed for pulse application at the inlet, whereas a concentration gradient of zero was set at a depth equal to infinity. The analytic solution provides values of $C_i(z, t; D_i)$ and $S_i(z, t; D_i)$, which are proportional to the influent concentration C_{i0} for colloids with diameter D_i. Values of $C_i(z, t; D_i)$ and $S_i(z, t; D_i)$ were divided by C_{i0} to obtain normalized concentrations (denoted as $C_i^*(z, t; D_i)$ and $S_i^*(z, t; D_i)$, respectively), which are independent of the influent colloid number.

Colloid filtration theory was used for k_i to reflect clean-bed conditions for retention (Yao et al., 1971) as:

$$k_i = \frac{3(1-\theta)}{2d_{50}}\eta_i \alpha v \tag{3}$$

where η_i [–] is the collector (porous medium) efficiency, α [–] is the colloid sticking efficiency, and d_{50} [L] is the median grain diameter of the porous medium. The value of η_i accounts for the mass flux of colloids with diameter D_i to the collector surface via diffusion,

interception, and gravitational sedimentation. It is defined as the ratio of the total colloid flux that strikes the collector (grain surface) to the rate at which particles flow toward the collector (Yao et al., 1971). Correlation equations to predict η_i as a function of system variables (water velocity, colloid size and density, and collector size) have been developed from pore-scale simulations of colloid transport in simplified grain geometries under water saturated conditions (e.g., Tufenkji and Elimelech, 2004; Messina et al., 2015). These correlation equations are strong functions of D_i. In this work, we employ the correlation equation of Messina et al. (2015) to estimate η_i.

The value of α in Eq. (3) is controlled by forces and torques that act on colloids near the SWI (Bradford and Torkzaban, 2015). The Brownian force arises from random fluctuation in the kinetic energy of diffusing colloids that is dependent on the solution temperature and colloid size (Ahmadi and Chen, 1998). Hydrodynamic forces and torque that act on a colloid adjacent to the SWI are dependent on the colloid size, the water velocity, the porosity, the grain size distribution, and the pore-space geometry (e.g., microscopic roughness and grain-grain contacts) (Bradford et al., 2011). Adhesive forces and torques are sensitive to a myriad of factors, including: solution chemistry, the surface properties and deformation of the SWI and colloid, and the size and amount of nanoscale roughness, microscopic roughness, and chemical heterogeneity (Bradford and Torkzaban, 2015). Many of the above factors that influence α are poorly characterized for colloids and porous media. Representative values of α were therefore selected for simulations discussed below to encompass commonly reported ranges in the literature (e.g., Ryan and Elimelech, 1996; Schijven and Hassanizadeh, 2000).

Colloid release under steady-state conditions is a slow, diffusion controlled process, and the release rate coefficient is typically several orders of magnitude smaller than the retention rate coefficient (Ryan and Elimelech, 1996). Very limited research has been directed to predicting the release rate coefficient under steady-state conditions (Johnson et al., 1995; Harter et al., 2000). Consequently, the value of k_{rs} was set to a low value of 0.001 min^{-1} that is typical for packed column studies (Bradford et al., 2016).

2.2. Stable polydispersed suspensions

A single value of D_i and k_i is used when simulating the transport and retention with Eqs. (1) and (2) for a monodispersed suspension. In the polydispersed modeling approach, the influent colloid size distribution is described using a probability distribution function, $f(D_i)$. The unimodal lognormal distribution function is given as:

$$f(D_i) = \frac{1}{D_i\sigma\sqrt{2\pi}} \exp\left[-\frac{(\ln(D_i) - \mu)^2}{2\sigma^2}\right] \tag{4}$$

where σ and μ are the standard deviation and mean value of the lognormal colloid size distribution, respectively. Note that $\mu = \ln(\langle D_i \rangle) - 0.5\sigma^2$, where $\langle D_i \rangle$ [L] is the ensemble average of D_i. Alternatively, a bimodal lognormal distribution function may be employed to describe more complex influent colloid size distributions as:

$$f(D_i) = \frac{\chi}{D_i\sigma_1\sqrt{2\pi}} \exp\left[-\frac{(\ln(D_i) - \mu_1)^2}{2\sigma_1^2}\right] + \frac{(1-\chi)}{D_i\sigma_2\sqrt{2\pi}} \exp\left[-\frac{(\ln(D_i) - \mu_2)^2}{2\sigma_2^2}\right] \tag{5}$$

where subscripts 1 and 2 identify two lognormal distributions and χ is the numerical fraction of colloids whose diameter is described by distribution 1.

The probability that a colloid in the influent suspension has a diameter less than or equal to D_i is given as:

$$F(D_i) = \int_0^{D_i} f(D)dD \tag{6}$$

where $F(D_i)$ is the cumulative distribution function evaluated at D_i, and D [L] is a dummy variable of integration for the colloid diameter. Note that $f(D_i)$ is equivalent to the fraction of colloids in the influent suspension:

$$f(D_i) = \frac{C_{i0}}{C_{T0}} \tag{7}$$

where C_{T0} [NL^{-3}] is the (total) influent colloid concentration.

The transport and retention of a stable, polydispersed colloid suspension may be quantified by the total aqueous (C_T, NL^{-3}) and solid (S_T, NM^{-1}) phase colloid concentrations at a given depth and time. Values of C_T and S_T can be obtained by integrating $C_i^*(z,t,D_i)$ and $S_i^*(z,t,D_i)$, respectively, over the full colloid size distribution as:

$$C_T(z,t) = C_{T0}\int_0^{\infty} f(D)C_i^*(z,t;D)dD \tag{8}$$

$$S_T(z,t) = C_{T0}\int_0^{\infty} f(D)S_i^*(z,t;D)dD \tag{9}$$

In this case, Eq. (7) is used to determine values of C_{i0} as $C_{T0}\,f(D_i)$.

Note that $F(D_i)$ (Eq. (6)) is independent of depth and time. In contrast, the dependency of retention on the colloid size changes the probability of obtaining a colloid of diameter less than D_i in the aqueous phase during transport, here denoted as $G(z, t; D_i)$. The value $G(z, t; D_i)$ is determined as:

$$G(z,t;D_i) = \frac{C_{T0}\int_0^{D_i} f(D)C_i^*(z,t;D)dD}{C_T(z,t)} \tag{10}$$

The numerator determines the aqueous phase concentration of colloids with a diameter less than or equal to D_i at a given depth and time.

It should be mentioned that aqueous and solid phase concentrations may be expressed by colloid mass instead of number by multiplying the right hand side of Eqs. (8)–(10) by the product of the colloid density and volume ($\pi {D_i}^3/6$) such that the integrand includes the ${D_i}^3$ term.

2.3. Aggregating polydispersed colloid suspensions

Colloids undergoing Brownian aggregation may be described using a time dependent lognormal colloid size distribution (Lee, 1983). In this case, the time-dependent total influent colloid concentration ($C_{T0}(t)$, NL^{-3}) is given as (Lee, 1983):

$$C_{T0}(t) = C_{T0}(0)[1 + \tau(1 + \exp(\sigma_0^2))]^{-1} \tag{11}$$

where σ_0 is the initial standard deviation of the lognormal colloid size distribution. The dimensionless aggregation time τ is given by $\alpha_a K t C_{T0}(0)$; where K [$L^3T^{-1}N^{-1}$] is the aggregation collision coefficient and α_a [–] is the aggregation sticking efficiency. The time dependent lognormal colloid size distribution, $f(D_i, t)$, is still given by Eq. (4), but now μ and σ are complex functions of σ_0 and τ that were derived by Lee (1983). Excellent agreement was obtained between predicted lognormal colloid size distributions with τ in this work and results presented by Lee (1983). Values of $C_{T0}(t)$ and $f(D_i, t)$ are predicted to decrease with time resulting in a larger spread in the colloid size distribution as τ increases.

The transport and retention of an aggregating colloid suspension was modeled as for stable suspension, with Eqs. (7)–(10), by

replacing C_{i0}, C_{T0} and $f(D_i)$ with $C_{i0}(t)$, $C_{T0}(t)$, and $f(D_i, t)$, respectively. In contrast to stable polydispersed colloid suspensions, aggregation causes aqueous and solid phase concentrations to decrease with time even when α=0 because of a decrease in $C_{T0}(t)$ and $f(D_i, t)$. This approach assumes that aggregation is independent of retention. This assumption is fully justified when α is low, but it may be violated when α increases because retention decreases the total number of colloids in the aqueous phase. Preliminary numerical experiments were conducted to assess the relative importance of this assumption by replacing $C_{T0}(0)$ in Eq. (11) with $C_T(z,t)$ for a stable polydispersed suspension (Eq. (8)). In this way the number of colloids in the aggregating suspension was reduced as retention increased. Direct inclusion of the effect of retention on aggregation in this manner only had a minor influence on predicted breakthrough curves and retention profiles and was not further considered. Aqueous and solid phase concentrations may be converted from colloid numbers to colloid mass in a similar manner as for a stable polydispersed suspension.

2.4. Numerical experiments

Stable and aggregating polydispersed suspension models were implemented into Microsoft Excel using Visual Basics for Applications programming language. Solutions of Eqs. (8)–(10) for stable polydispersed suspensions require knowledge of $f(D_i)$, $k_i(D_i)$, $C_i^*(z,t;D_i)$, and $S_i^*(z,t;D_i)$ for a given value of D_i. The value of $f(D_i)$ was obtained using Eqs. (4) or (5), whereas $k_i(D_i)$ was determined using Eq. (3) and the correlation equation of Messina et al. (2015). Values of $C_i^*(z,t;D_i)$ and $S_i^*(z,t;D_i)$for a given $k_i(D_i)$ where acquired using CXTFIT (Tang et al., 2010). Integrals were evaluated numerically with respect to D_i using the m-point Gauss–Chebyshev quadrature formula (e.g., Carnahan et al., 1969). A similar approach was applied for aggregating polydispersed suspensions. In this case, $f(D_i)$ was replaced by $f(D_i, t)$ which was determined using the approach of Lee (1983). It should be mentioned that this method only considers changes in the colloid size distribution with respect to time, but it does not differentiate between a single colloid and an aggregate that has a size of D_i.

Numerical experiments were conducted to investigate the influence of colloid size distribution parameters on transport and retention. Simulations for a monodispersed colloid suspension were conducted to examine the influence of average D_i and k_i on colloid migration behavior. Simulations of stable polydispersed suspensions with a unimodal lognormal colloid size distribution probed the roles of σ and $\langle D_i \rangle$, whereas those with a bimodal lognormal size distribution explored the influence of χ. The influence of aggregation was investigated for different values of α and $C_{T0}(0)$. Values of pertinent model parameters are given in the figure captions.

Simulated colloid breakthrough curves (BTCs) and final retention profiles (RPs) were determined for a 4 pore volume input pulse. BTCs and RPs are given at a depth of 10 cm and after 8 pore volumes (vt/L_D), respectively, to facilitate the visualization of colloid concentrations. The BTCs were plotted with the relative concentration (C_i/C_{i0} for monodispersed suspension, C_T/C_{T0} for a stable polydispersed suspension, and $C_T/C_{T0}(0)$ for an aggregating polydispersed suspension) on the vertical axis and the pore-volume number on the horizontal axis, whereas semi-log plots of the RPs are given with the normalized solid phase colloid concentration (S/C_{i0} for monodispersed suspensions, S_T/C_{T0} for a stable polydispersed suspension, and $S_T/C_{T0}(0)$ for an aggregating polydispersed suspension) on the vertical log axis and depth on the horizontal axis. Values of $G(z, t; D_i)$ were determined for the full range of D_i in the colloid distribution when t = 100 min and z = 1, 2, 4, 6, and 10 cm.

3. Results and discussion

3.1. Monodispersed colloid suspensions

Fig. 1 presents the predicted influence of D_i on k_i (min^{-1}) when using filtration theory in which d_{50} = 360 μm, θ = 0.34, the Darcy velocity (q) = 0.1 cm min^{-1}, α = 1, and the colloid density = 1.08 g cm^{-3}. Note that k_i achieves a minimum when D_i is approximately 1500 nm, and this reflects the optimum colloid size for transport (the lowest rate of mass transfer to the SWI) under the considered condition. The relative importance of mass transfer

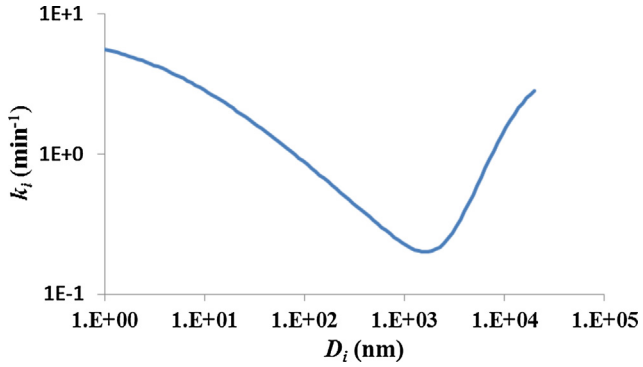

Fig. 1. Log plots of the predicted influence of colloid diameter (D_i) on k_i when using filtration theory (Eq. (3)) and the correlation equation of Messina et al. (2015). The value of d_{50} = 360 μm, θ = 0.34, q = 0.1 cm min^{-1}, α = 1, and the colloid density = 1.08 g cm^{-3}.

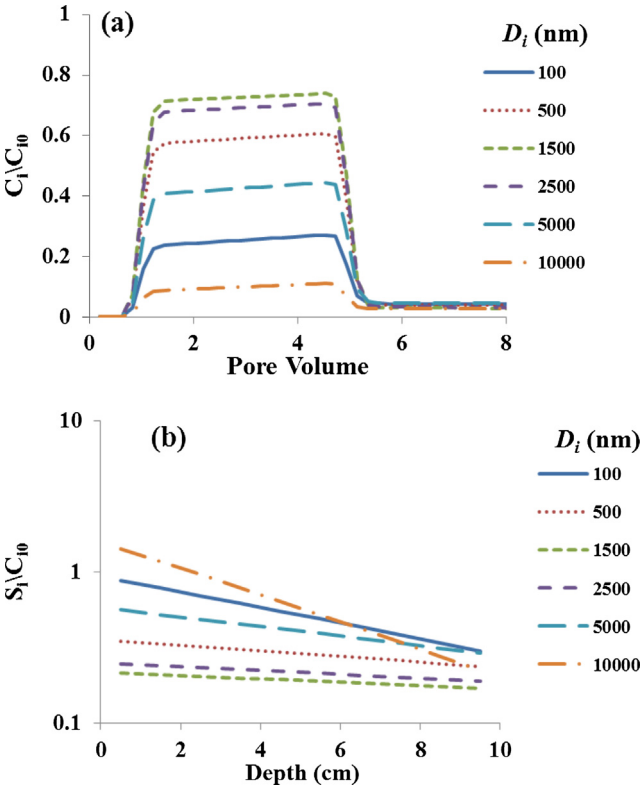

Fig. 2. Simulated BTCs and RPs for a monodispersed colloid suspension when using filtration theory (Eq. (3)), D_i = 100, 500, 1500, 2500, 5000, and 10000 nm, d_{50} = 360 μm, θ = 0.34, q = 0.1 cm min^{-1}, α = 0.05, and the colloid density = 1.08 g cm^{-3}.

by sedimentation, interception, and diffusion changes with the colloid size. Sedimentation and interception increase for larger D_i, whereas diffusion plays a larger role for smaller D_i. In addition to D_i, the value of k_i is also predicted to depend on d_{50}, q, and the colloid density. The interested reader is referred to the literature for further discussion of these topics (Tufenkji and Elimelech, 2004; Messina et al., 2015).

Fig. 2a and b presents illustrative examples of the predicted influence of D_i (100, 500, 1500, 2500, and 5000 nm) on BTCs and RPs, respectively, when d_{50} = 360 μm, θ = 0.34, q = 0.1 cm min^{-1}, α = 0.05, and the colloid density = 1.08 g cm^{-3}. Values of k_i change with D_i in a similar manner to that shown in Fig. 1. The smallest amount of retention occurred in Fig. 2 when D_i = 1500 nm because k_i and the mass transfer rate was smallest under this condition (Fig. 1). Conversely, lower breakthrough concentrations and greater amounts of retention occur for smaller and larger colloid sizes due to greater mass transfer rates to the SWI.

It should be mentioned that filtration theory predictions of colloid transport with size (Figs. 1 and 2) are well known in the literature (e.g., Ryan and Elimelech, 1996; Tufenkji and Elimelech, 2004). This information is included to aid in the interpretation of simulations for stable or aggregating polydispersed colloid suspensions that are discussed below.

3.2. Stable polydispersed colloid suspensions

This section discusses simulated transport and retention behavior for various stable polydispersed colloid suspensions. Fig. 3a and b present illustrative examples of predicted BTCs and RPs when the colloids were lognormally distributed with an initial $\langle D_i \rangle$ = 1500 nm and σ = 0.1, 1, and 2. Other simulation conditions included a d_{50} = 360 μm, θ = 0.34, q = 0.1 cm min^{-1}, α = 0.05, and the colloid density = 1.08 g cm^{-3}. Increases in σ produced greater amounts of colloid retention, with a decrease in the peak value of C_T/C_{T0} and an increase in S_T/C_{T0}. This observation reflects the composite effects of D_i on colloid retention shown in Fig. 1. In particular, increasing deviation from the optimum transport value of D_i = 1500 nm produces greater amounts of retention. However, it should be mentioned that increasing σ will not always influence C_T/C_{T0} and S_T/C_{T0} in the same manner as shown in Fig. 3. Fig. 1 indicates that k_i changes in a nonmonotonic fashion with D_i. In some cases increasing σ may actually produce a decrease in retention (higher peak values of C_T/C_{T0} and a decrease in S_T/C_{T0}); e.g., Fig. 4 shows such an example when the initial $\langle D_i \rangle$ = 10000 nm.

Eqs. (1) and (2) predict an exponential decrease in the retained colloid concentration with distance when k_{rs} is small. In contrast, many experimental observations have reported that retention profiles decrease with distance in a hyper-exponential manner (Chatterjee and Gupta, 2009; Bradford et al., 2014); e.g., the value of $\log(S_T/C_{T0})$ is greater than linear with depth at the inlet. This hyper-exponential behavior has previously been attributed to a polydispersed colloid size distribution (Chatterjee and Gupta, 2009). Indeed, values of S_T/C_{T0} shown in Fig. 3b exhibit increasing deviation from exponential behavior with increasing σ. Furthermore, Fig. 5 indicates that the RPs become increasingly hyper-exponential with increasing α for a given σ.

Additional simulations were conducted to better understand the influence of transport and retention on changes in the aqueous phase colloid size distribution. Fig. 6a–c present plots of the $G(z, t; D_i)$ as a function of D_i when z = 1, 2, 4, 6, and 10 cm, t = 100 min,

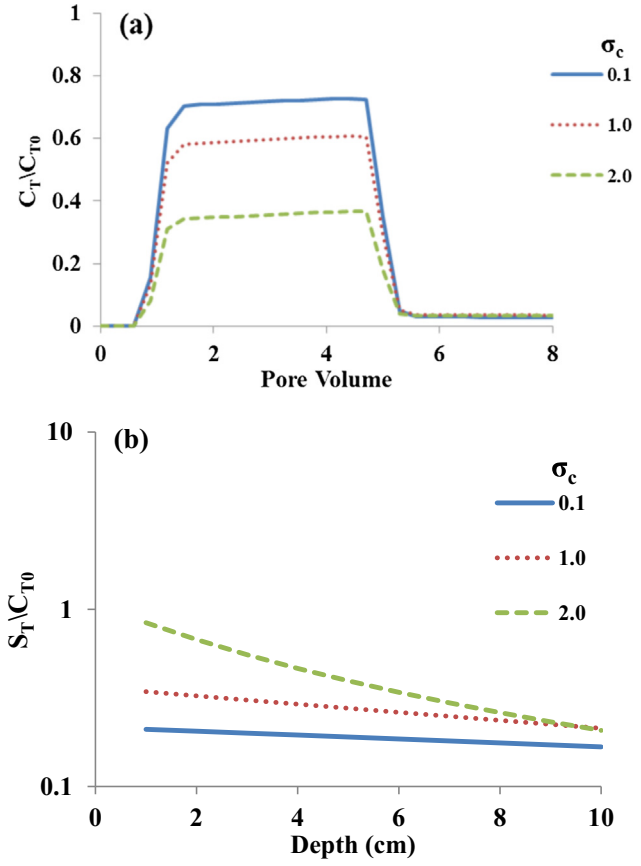

Fig. 3. Simulated BTCs and RPs for a stable polydispersed suspension when colloids are lognormally distributed with σ = 0.1, 1, and 2, $\langle D_i \rangle$ = 1500 nm, d_{50} = 360 μm, θ = 0.34, q = 0.1 cm min^{-1}, α = 0.05, and colloid density = 1.08 g cm^{-3}.

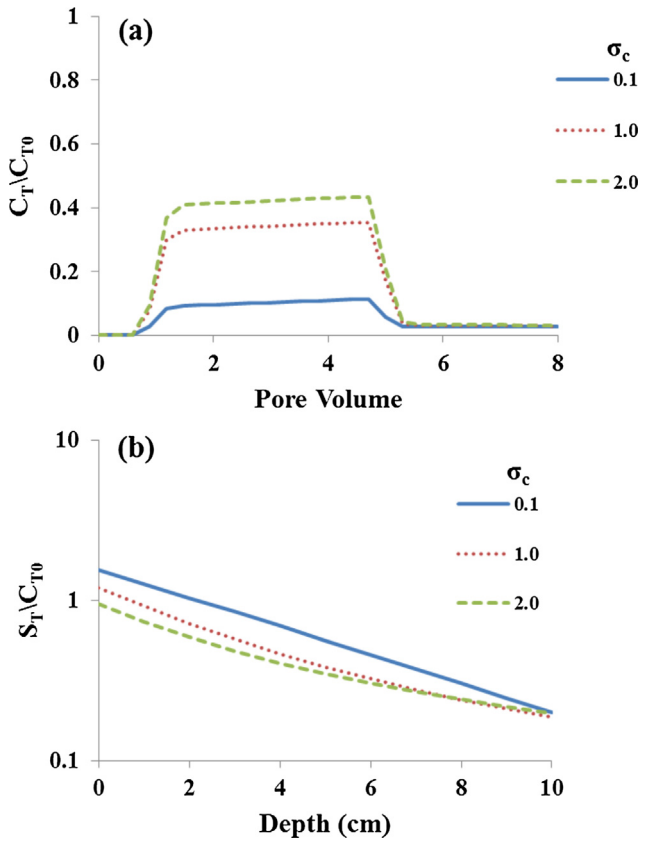

Fig. 4. Simulations of BTCs and RPs for a stable polydispersed suspension when colloids are lognormally distributed with σ = 0.1, 1, and 2, $\langle D_i \rangle$ = 10000 nm, d_{50} = 360 μm, θ = 0.34, q = 0.1 cm min^{-1}, the colloid density = 1.08 g cm^{-3}, and α = 0.05.

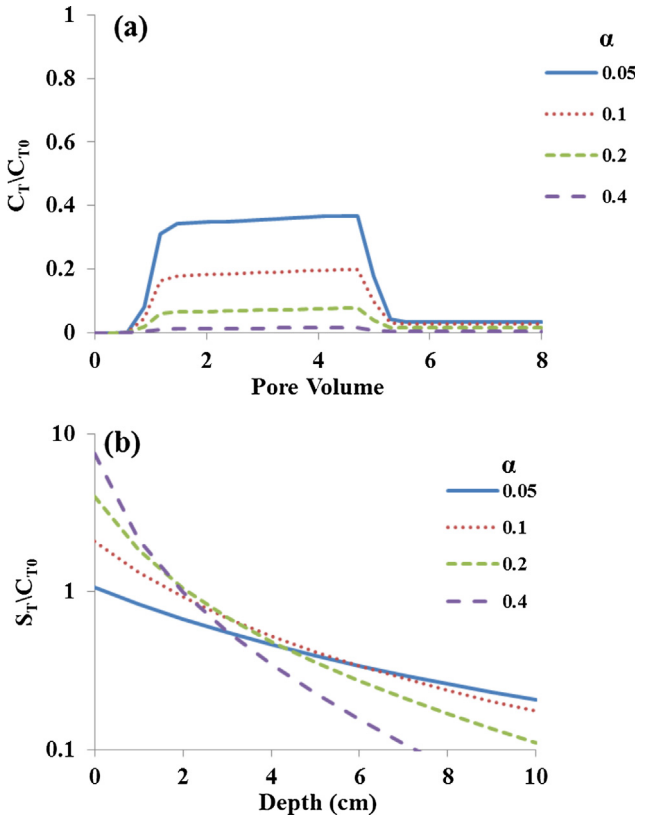

Fig. 5. Simulations of BTCs and RPs for a stable polydispersed suspension when colloids are lognormally distributed with $\sigma = 2$, $\langle D_i \rangle = 1500$ nm, $d_{50} = 360$ μm, $\theta = 0.34$, $q = 0.1$ cm min^{-1}, the colloid density = 1.08 g cm^{-3}, and $\alpha = 0.05$, 0.1, 0.2, and 0.4.

$\sigma = 1$, and $\langle D_i \rangle = 100$, 1000, and 10000 nm. Other simulations conditions were the same as in Fig. 3. Similar to $F(D_i)$ for the influent suspension, $G(z, t; D_i)$ is the probability that transported colloids in the aqueous phase will be smaller than D_i. In all cases, $G(z, t; D_i)$ becomes more uniform with increasing transport distance, and the median value of the distribution approaches 1500 nm as expected from Fig. 1. The smallest changes in $G(z, t; D_i)$ occurred with transport when $\langle D_i \rangle = 1000$ nm, because $G(z, t; D_i)$ was close to the optimum conditions for transport. In contrast, lower and higher portions of $G(z, t; D_i)$ were more rapidly removed when $\langle D_i \rangle = 100$ and 10000 nm, respectively. This observation suggests that transport of stable polydispersed colloid suspensions is of primary importance near the soil surface.

A single lognormal distribution (Eq. (4)) may be inadequate to describe all colloid size distributions. The bimodal lognormal distribution (Eq. (5)) provides higher flexibility to describe more complex colloid size distributions in the influent. Fig. 7a and b presents illustrative examples of the predicted values of BTCs and RPs when the colloid sizes are described using a bimodal lognormal distributed with an initial $\langle D_{i1} \rangle = 100$ nm, $\langle D_{i2} \rangle = 3000$ nm, $\sigma_1 = 0.1$, $\sigma_2 = 0.5$, and $\chi = 0$, 0.25, 0.5, 0.75, and 1. Other simulation conditions were the same as in Fig. 3. Increasing χ produces decreasing amounts of colloid breakthrough (Fig. 7a) and increasing amounts of retention (Fig. 7b) because smaller colloids in distribution 1 were more efficiently removed than larger colloids in distribution 2 (Fig. 1).

Fig. 8 presents plots of $G(z, t; D_i)$ as a function of D_i when $z = 1$, 2, 4, 6, and 10 cm, $t = 100$ min, the initial $\langle D_{i1} \rangle = 100$ nm, $\langle D_{i2} \rangle = 3000$ nm, $\sigma_1 = 0.1$, $\sigma_2 = 0.5$, and $\chi = 0.5$. Other simulation conditions were the same as in Fig. 3. As anticipated, changes in $G(z, t; D_i)$ with increasing transport distance were more

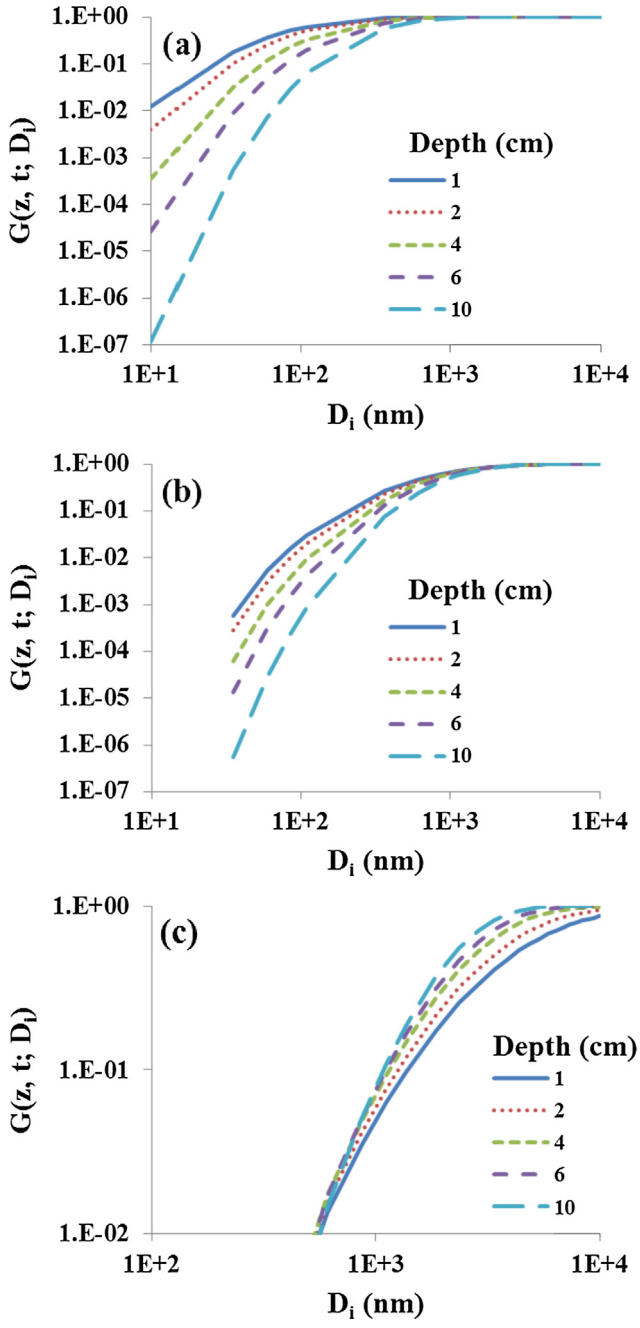

Fig. 6. Log-log plots of $G(z, t; D_i)$ as a function of D_i at $z = 1$, 2, 4, 6, and 10 cm for a stable polydispersed colloid suspension when $t = 100$ min, $\langle D_i \rangle = 100$ (a), 1000 (b), and 10,000 (c) nm, $\sigma = 1$, $d_{50} = 360$ μm, $\theta = 0.34$, $q = 0.1$ cm min^{-1}, $\alpha = 0.2$, and colloid density = 1.08 g cm^{-3}.

pronounced when using a bimodal than a unimodal lognormal distribution (comparison of Figs. 8 and 6) because the smaller colloids were removed more rapidly than the larger sized colloids (Fig. 1).

3.3. Aggregating colloid suspensions

The simulated influence of aggregation is investigated in this section. Fig. 9a and 9b present plots of BTCs and RPs when an aggregating colloid suspension is lognormally distributed with an initial $\langle D_i \rangle = 1000$ nm and $\sigma_0 = 0.7$, $d_{50} = 360$ μm, $q = 0.1$ cm min^{-1}, $C_{T0}(0) = 10^8$ N ml^{-1}, $\alpha_a = 1.0$, and $\alpha = 0$, 0.01, 0.05, 0.1, and 0.2. Note that values of $C_T/C_{T0}(0)$ decrease with increasing colloid injection time after breakthrough (Fig. 9a). This behavior has typically been

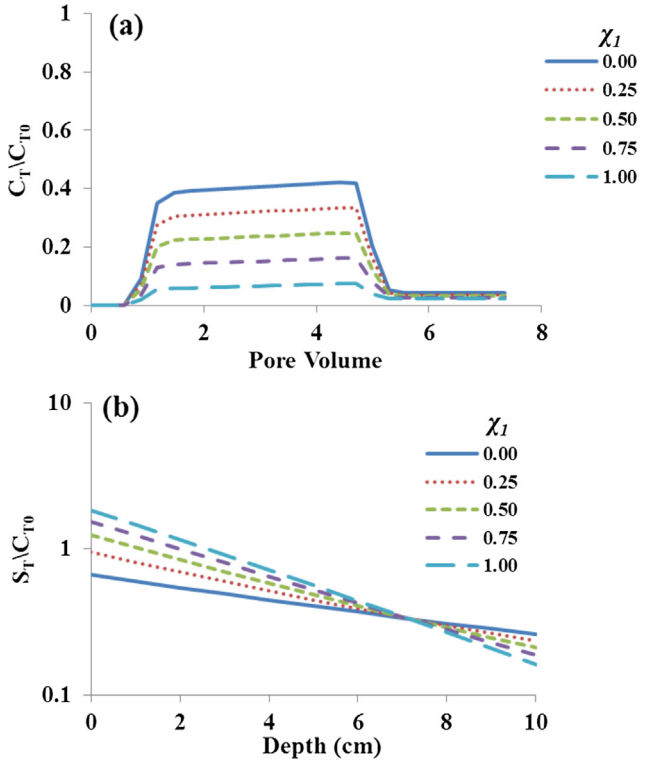

Fig. 7. Simulated BTCs and RPs for a stable polydispersed suspension when a bimodal lognormal distribution was used to describe the colloids with $\langle D_{i1}\rangle$ = 100 nm, $\langle D_{i2}\rangle$ = 3000 nm, σ_1 = 0.1, σ_2 = 0.5, and χ = 0, 0.25, 0.5, 0.75, and 1, d_{50} = 360 μm, θ = 0.34, q = 0.1 cm min^{-1}, α = 0.05, and colloid density = 1.08 g cm^{-3}.

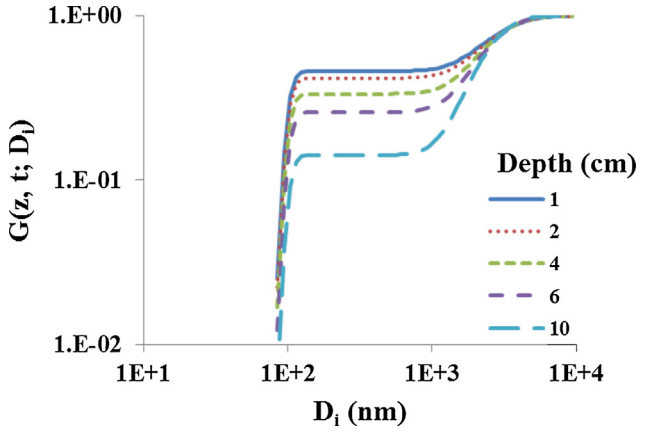

Fig. 8. Log-log plots of $G(z, t; D_i)$ as a function of D_i at z = 1, 2, 4, 6, and 10 cm for a stable polydispersed colloid suspension when using a bimodal lognormal distribution with t = 100 min, $\langle D_{i1}\rangle$ = 100 nm, $\langle D_{i2}\rangle$ = 3000 nm, σ_1 = 0.1, σ_2 = 0.5, χ = 0.5, d_{50} = 360 μm, θ = 0.34, q = 0.1 cm min^{-1}, α = 0.1, and the colloid density = 1.08 g cm^{-3}.

ascribed to "ripening"; i.e., retained colloids acting as favorable sites for subsequent colloid retention. Fig. 9a indicates that this "ripening" behavior may also be attributed to aggregation of the colloid suspension during transport. Note that aggregation has a dominant influence on breakthrough behavior when the retention rate is minimal (small α). Conversely, as the retention rate increases (larger α) the relative influence of aggregation on the breakthrough curve becomes less apparent. This occurs because retention decreases the peak value of the breakthrough curve and the colloid size distribution tends to be more uniform with increasing distance as a result of differences in the retention

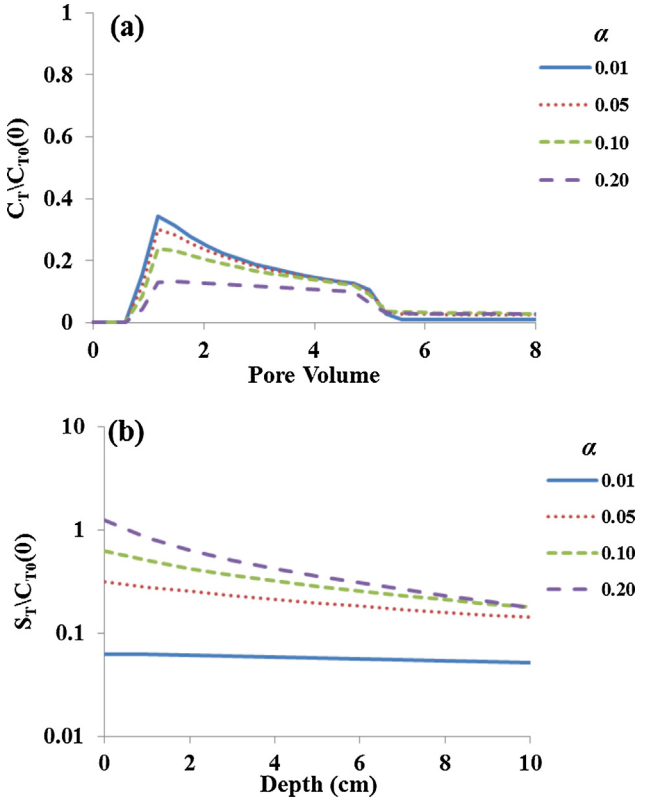

Fig. 9. Simulated BTCs and RPs for a aggregating polydispersed suspension when colloids are lognormally distributed with $\langle D_i\rangle$ = 1000 nm and σ_0 = 0.7, d_{50} = 360 μm, q = 0.1 cm min^{-1}, $C_{T0}(0)$ = 10^8N ml^{-1}, α_a = 1.0, and α = 0.01, 0.05, 0.10, and 0.20.

behavior with colloid size (Figs. 1 and 6). Aggregation has a smaller influence on the retention profiles than α; e.g., increasing α produce greater amounts of retention.

Fig. 10a and b presents plots of BTCs and RPs for an aggregating colloid suspension with a colloid size that is lognormally distributed with an initial $\langle D_i\rangle$ = 1500 nm and σ_0 = 0.7, α_a = 1.0, α = 0.05, and $C_{T0}(0)$ = 10^5, 10^6, 10^7, 10^8, and 10^9 N ml^{-1}. Similar to Fig. 9a, aggregation produces a decrease in the value of $C_T/C_{T0}(0)$ with increasing colloid injection time after breakthrough. Note, however, that the rate of decrease in $C_T/C_{T0}(0)$ is a strong function of the initial value of $C_{T0}(0)$. Recall that $C_{T0}(t)$ decreases more rapidly with increasing $C_{T0}(0)$ (Eq. (11)). Consequently, the peak value of $C_T/C_{T0}(0)$ also decreases more rapidly with increasing $C_{T0}(0)$ because of greater aggregation. The retention profile is determined by the constant value of α and changes in $C_T/C_{T0}(0)$ shown in Fig. 10a. The maximum value of $S_T/C_{T0}(0)$ occurs when $C_T/C_{T0}(0)$ is maximum and aggregation is minimum. Smaller values of $S_T/C_{T0}(0)$ occur for higher $C_{T0}(0)$ at deeper transport distances because of lower $C_T/C_{T0}(0)$ due to greater aggregation. In addition, the retention profiles become more hyper-exponential with increasing $C_{T0}(0)$. This implies that aggregation primarily influenced transport behavior at shallower transport distances. This finding is supported by observations shown in Fig. 9b for higher values of α.

A few final remarks about aggregating colloid suspensions are given below. Increasing the initial σ_0 had a similar influence on the breakthrough curves and retention profiles as for the stable polydispersed suspensions shown in Fig. 3. However, the retention profiles become more hyper-exponential with aggregating suspensions and increasing dimensionless aggregation time (Fig. 10b). Similar to stable polydispersed suspensions, the aggregating suspensions primarily influenced retention behavior near the soil

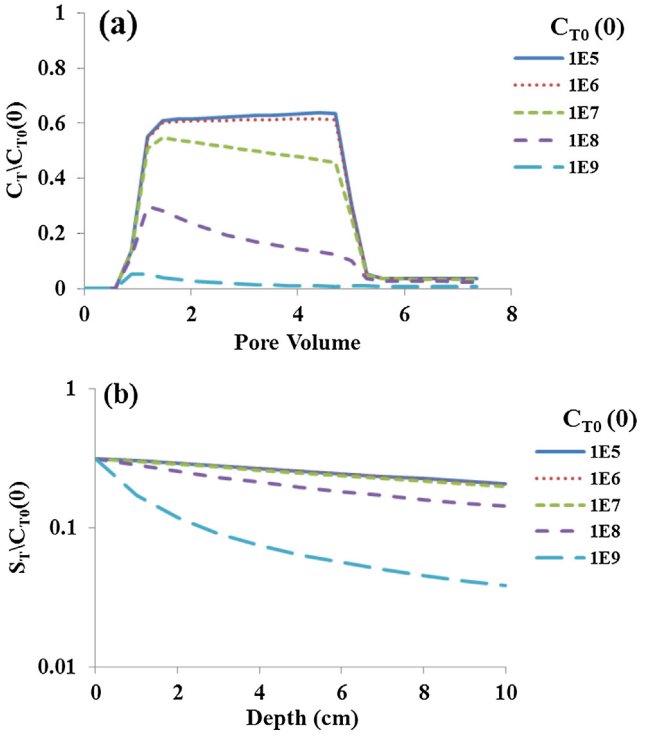

Fig. 10. Simulated BTCs and RPs for an aggregating polydispersed suspension when colloids are lognormally distributed with $\langle D_i \rangle$ = 1500 nm and σ_0 = 0.7, d_{50} = 360 μm, q = 0.1 cm min^{-1}, α_a = 1.0, α = 0.05, and $C_{T0}(0) = 10^5$, 10^6, 10^7, 10^8, and 10^9 N ml^{-1}.

surface and $G(z, t; D_i)$ became more uniform with increasing transport distance. Aggregation during transport becomes more apparent when retention is minimal; e.g., for small values of α and for initial $\langle D_i \rangle$ values that are optimal for transport. In addition, the above dependency of aggregation on C_{T0} and time can also be reduced by multiplying the Brownian collision efficiency by smaller values of α_a, such that only a fraction of the Brownian collisions lead to aggregation.

4. Summary and conclusions

Most models to describe colloid transport and fate in the subsurface have been developed for mono-dispersed suspensions, whereas natural systems typically exhibit a wide distribution of colloid sizes. A mathematical model was developed to describe the transport and retention of a stable or aggregating polydispersed colloid suspension in porous media. The initial colloid size distribution was described using a unimodal lognormal or a bimodal lognormal PDF. Brownian aggregation was accounted for in the model by making the parameters of the lognormal PDF a function of time. The transport and retention of a given sized colloid was described using an analytical solution that considers advective and dispersive colloid transport, and first-order retention and release. Colloid filtration theory was included in the model to predict the dependence of the colloid retention coefficient on parameters such as colloid size and density, water velocity, and grain size. The total suspension concentration was determined by integrating the product of the individual concentration of a given colloid size and the PDF over the complete colloid size distribution. Changes in the colloid size distribution during transport at a specific location and time were determined from the calculated cumulative colloid size distribution function.

Filtration theory predicts an optimum size for colloid transport of around 955–1700 nm depending on velocity, grain size, and the colloid density. Colloids that are smaller or larger than this size range are removed more efficiently. Consequently, the amount of retention of a polydispersion suspension is highly dependent on the size distribution parameters. When $\langle D_i \rangle$ of a lognormal distribution is close to the optimum size range for transport, increasing σ produces greater amounts of retention and more hyper-exponential retention profiles. In contrast, when $\langle D_i \rangle$ is smaller or larger than the optimum transport size then increasing σ may sometimes produce a decrease in retention. Similar trends were obtained when using a bimodal lognormal colloid size distribution, but with an increased sensitivity to distribution properties. Aggregation produces a similar decrease in the breakthrough concentrations with injection time as ripening because of a decrease in $C_{T0}(t)$ and $f(D_i, t)$, especially when α was low. This aggregation effect was much more pronounced at higher input concentration levels, which also produced retention profiles that were increasingly hyper-exponential. Simulation results indicate that the colloid size distribution of stable and aggregating suspensions always becomes more uniform and approaches the optimum transport size with increasing distance, suggesting that consideration of polydispersed suspensions is of primary importance near the injection surface. Consequently, polydispersed suspensions are expected to contribute to the development of clogging that is commonly observed at these locations. Future research will expand the developed model to account for the influence of polydispersed suspensions on clogging.

Acknowledgements

This research was supported by the USDA, ARS, National Program 211.

References

Ahmadi, M., Chen, Q., 1998. Dispersion and deposition of particles in a turbulent pipe flow with sudden expansion. J. Aerosol Sci. 29, 1097–1116.
Alem, A., Elkawafi, A., Ahfir, N.D., Wang, H.Q., 2013. Filtration of kaolinite particles in a saturated porous medium: hydrodynamic effects. Hydrogeol. J. 21, 573–586.
Alem, A., Ahfir, N.D., Elkawafi, A., Wang, H.Q., 2015. Hydraulic operating conditions and particle concentration effects on physical clogging of a porous medium. Transp. Porous Media 106, 303–321.
Bian, S.W., Mudunkotuwa, I.A., Rupasinghe, T., Grassian, V.H., 2011. Aggregation and dissolution of 4 nm ZnO nanoparticles in aqueous environments: Influence of ph, ionic strength, size, and adsorption of humic acid. Langmuir 27, 6059–6068.
Bradford, S.A., Kim, H., Headd, B., Torkzaban, S., 2016. Evaluating the transport of *Bacillus subtilis* spores as a potential surrogate for *Cryptosporidium parvum* oocysts. Environ. Sci. Technol. 50, 1295–1303.
Bradford, S.A., Tadassa, Y.F., Pachepsky, Y., 2006. Transport of *Giardia* and manure suspensions in saturated porous media. J. Environ. Qual. 35, 749–757.
Bradford, S.A., Toride, N., 2007. A stochastic model for colloid transport and deposition. J. Environ. Qual. 36, 1346–1356.
Bradford, S.A., Torkzaban, S., Wiegmann, A., 2011. Pore-scale simulations to determine the applied hydrodynamic torque and colloid immobilization. Vadose Zone J. 10, 252–261.
Bradford, S.A., Torkzaban, S., 2015. Determining parameters and mechanisms of colloid retention and release in porous media. Langmuir 31, 12096–12105.
Bradford, S.A., Wang, Y., Kim, H., Torkzaban, S., Šimůnek, J., 2014. Modeling microorganism transport and survival in the subsurface. J. Environ. Qual. 43, 421–440.
Carnahan, B., Luther, H.A., Wilkes, J.O., 1969. Applied Numerical Models. John Wiley, New York.
Chatterjee, J., Abdulkareem, S., Gupta, S.K., 2010. Estimation of colloidal deposition from heterogeneous populations. Water Res. 44, 3365–3374.
Chatterjee, J., Gupta, S.K., 2009. An agglomeration-based model for colloid filtration. Environ. Sci. Technol. 43, 3694–3699.
Chang, J.S., Vigneswaran, S., 1990. Mathematical modelling of the effect of size distribution on suspended particles in deep-bed filtration. Aqua 39, 96–100.
Chen, G.X., Liu, X.Y., Su, C.M., 2011. Transport and retention of TiO2 rutile nanoparticles in saturated porous media under low-ionic-strength conditions: Measurements and mechanisms. Langmuir 27, 5393–5402.
Elimelech, M., Gregory, J., Jia, X., 2013. Particle deposition and aggregation: measurement, modelling and simulation. Butterworth-Heinemann.

Fang, J., Shan, X., Wen, B., Lin, J., Owens, G., 2009. Stability of titania nanoparticles in soil suspensions and transport in saturated homogeneous soil columns. Environ. Sci. Technol. 157, 1101–1109.

Filella, M., Zhang, J., Newman, M.E., Buffle, J., 1997. Analytical applications of photon correlation spectroscopy for size distribution measurements of natural colloidal suspensions: capabilities and limitations. Coll. Surf. A: Physicochem. Eng. Aspects 120, 27–46.

Harter, T., Wagner, S., Atwill, E.R., 2000. Colloid transport and filtration of Cryptosporidium parvum in sandy soils and aquifer sediments. Environ. Sci. & Technol. 34, 62–70.

Jiang, X.J., Tong, M.P., Lu, R.Q., Kim, H., 2012. Transport and deposition of ZnO nanoparticles in saturated porous media. Coll. Surf. A: Physicochem. Eng. Aspects 401, 29–37.

Johnson, W.P., Blue, K.A., Logan, B.E., Arnold, R.G., 1995. Modeling bacterial detachment during transport through porous media as a residence-time-dependent process. Water Resour. Res. 31, 2649–2658.

Klaine, S.J., Alvarez, P.J.J., Batley, G.E., Fernandes, T.F., Handy, R.D., Lyon, D.Y., Mahendra, S., McLaughlin, M.J., Lead, J.R., 2008. Nanomaterials in the environment: Behavior, fate, bioavailability, and effects. Environ. Toxicol. Chem. 27, 1825–1851.

Lee, K.W., 1983. Change of particle size distribution during Brownian coagulation. J. Coll. Interf. Sci. 92, 315–325.

Mackie, R.I., Zhao, Q., 1999. A framework for modelling removal in the filtration of polydisperse suspensions. Water Res. 33, 794–806.

Messina, F., Marchisio, D.L., Sethi, R., 2015. An extended and total flux normalized correlation equation for predicting single-collector efficiency. J. Coll. Interf. Sci. 446, 185–193.

Raychoudhury, T., Tufenkji, N., Ghoshal, S., 2012. Aggregation and deposition kinetics of carboxymethyl cellulose-modified zero-valent iron nanoparticles in porous media. Water Res. 46, 1735–1744.

Ryan, J.N., Elimelech, M., 1996. Colloid mobilization and transport in groundwater. Coll. Surf. A: Physicochem. Eng. Aspects 107, 1–56.

Schaap, M.G., Leij, F.J., van Genuchten, M.Th., 2001. ROSETTA: a computer program for estimating soil hydraulic parameters with hierarchical pedotransfer functions. J. Hydrol. 251, 163–176.

Schijven, J.F., Hassanizadeh, S.M., 2000. Removal of viruses by soil passage: Overview of modeling, processes, and parameters. Crit. Rev. Environ. Sci. Technol. 30, 49–127.

Solovitch, N., Labille, J., Rose, J., Chaurand, P., Borschneck, D., Wiesner, M.R., Bottero, J.Y., 2010. Concurrent aggregation and deposition of TiO2 nanoparticles in a sandy porous media. Environ. Sci. Technol. 44, 4897–4902.

Taghavy, A., Pennell, K.D., Abriola, L.M., 2015. Modeling coupled nanoparticle aggregation and transport in porous media: A Lagrangian approach. J. Contam. Hydrol. 172, 48–60.

Tang, G., Mayes, M.A., Parker, J.C., Jardine, P.M., 2010. CXTFIT/Excel–A modular adaptable code for parameter estimation, sensitivity analysis and uncertainty analysis for laboratory or field tracer experiments. Comput. Geosci. 36, 1200–1209.

Toride, N., Leij, F.J., van Genuchten, M.T., 1995. The CXTFIT Code for Estimating Transport Parameters from Laboratory or Filed Tracer Experiments. US Salinity Laboratory, Riverside.

Tufenkji, N., Elimelech, M., 2004. Correlation equation for predicting single-collector efficiency in physicochemical filtration in saturated porous media. Environ. Sci. Technol. 38, 529–536.

Tufenkji, N., Redman, J.A., Elimelech, M., 2003. Interpreting deposition patterns of microbial particles in laboratory-scale column experiments. Environ. Sci. Technol. 37, 616–623.

Vigneswaran, S., Chang, J.S., Janssens, J.G., 1990. Experimental investigation of size distribution of suspended particles in granular bed filtration. Water Res. 24, 927–930.

Wang, Y., Gao, B., Morales, V.L., Tian, Y., Wu, L., Gao, J., Bai, W., Yang, L., 2012a. Transport of titanium dioxide nanoparticles in saturated porous media under various solution chemistry conditions. J. Nanopart. Res. 14, 1095–1104.

Wang, D.J., Bradford, S.A., Harvey, R.W., Gao, B., Cang, L., Zhou, D.M., 2012b. Humic acid facilitates the transport of ARS-labeled hydroxyapatite nanoparticles in iron oxyhydroxide-coated sand. Environ. Sci. Technol. 46, 2738–2745.

Wiesner, M.R., Bottero, J.-Y., 2007. Environmental Nanotechnology. The McGraw-Hill Companies, New York, p. 540.

Yao, K.M., Habibian, M.T., O'Melia, C.R., 1971. Water and waste water filtration. Concepts and applications. Environ. Sci. Technol. 5, 1105–1112.